HHS Public Access

Author manuscript

Gastroenterology. Author manuscript; available in PMC 2019 May 01.

Published in final edited form as:

Gastroenterology. 2018 May ; 154(6): 1805–1821.e5. doi:10.1053/j.gastro.2018.01.025.

Pancreatitis-Induced Depletion of Syntaxin 2 Promotes Autophagy and Increases Basolateral Exocytosis

Subhankar Dolai[1,§], **Tao Liang**[1], **Abrahim I. Orabi**[3], **Douglas Holmyard**[4], **Li Xie**[1], **Dafna Greitzer-Antes**[1], **Youhou Kang**[1], **Huanli Xie**[1], **Tanveer A. Javed**[3], **Patrick P. Lam**[1], **Deborah C. Rubin**[5], **Peter Thorn**[6], and **Herbert Y. Gaisano**[1,2,§]

[1]Department of Medicine, University of Toronto, Toronto, Ontario, Canada

[2]Department of Physiology, University of Toronto Toronto, Ontario, Canada

[3]Children's Hospital of Pittsburgh of University of Pittsburgh Medical Center, Pittsburgh, Pennsylvania

[4]Lunenfeld-Tanenbaum Research Institute, Mount Sinai Hospital, Toronto, Canada

[5]Division of Gastroenterology, Departments of Medicine, and Developmental Biology, Washington University School of Medicine, St Louis Missouri

[6]University of Sydney, Sydney, New South Wales, Australia

Abstract

BACKGROUND & AIMS: Pancreatic acinar cells are polarized epithelial cells that store enzymes required for digestion as inactive zymogens, tightly packed at the cell apex. Stimulation of acinar cells causes the zymogen granules to fuse with the apical membrane, and the cells undergo exocytosis to release proteases into the intestinal lumen. Autophagy maintains homeostasis of pancreatic acini. Syntaxin 2 (STX2), an abundant soluble N-ethyl maleimide sensitive factor attachment protein receptor in pancreatic acini, has been reported to mediate apical exocytosis. Using human pancreatic tissues and STX2-knockout (KO) mice, we investigated the functions of STX2 in zymogen granule-mediated exocytosis and autophagy.

Address requests for reprints to: Herbert Y. Gaisano, MD, Department of Medicine, University of Toronto, Room 7368, Medical Sciences Building, 1 King's College Circle, Toronto, Ontario, M5S 1A8, Canada. herbert.gaisano@utoronto.ca; fax: (416) 978-8765. Subhankar Dolai, PhD, Department of Medicine, University of Toronto, Room 7368, Medical Sciences Building, 1 King's College Circle. Toronto, Ontario, M5S 1A8, Canada. subhankar.dolai@gmail.com; fax: (416) 978-8765.

§Authors share co-senior authorship.

Author contributions: H.Y.G. and S.D. formulated the original hypothesis and co-wrote the manuscript. S.D. performed acini immunofluorescence, exocytosis imaging, enzyme assays, and binding experiments. S.D., A.I.O., and T.A.J. performed the pancreatitis experiments. S.D. and P.T. performed the calcium studies. S.D., T.L., and LX performed the human pancreas slicing and imaging. D.H. carried out electron microscopy. Y.K. performed the reverse transcription polymerase chain reaction. H.X. purified recombinant proteins. D.G.-A. provided help in computational analyses. D.C.R. provided the Syntaxin-2-KO mice and total RNA from mouse small intestinal myofibroblasts. All authors discussed the results and revised the manuscript. H.Y.G. is the guarantor of this work and, as such, had full access to all the data in the study and takes responsibility for the integrity of the data and the accuracy of the data analysis.

Conflicts of interest

The authors disclose no conflicts.

Supplementary Material

Note: To access the supplementary material accompanying this article, visit the online version of *Gastroenterology* at www.gastrojournal.org, and at https://doi.org/10.1053/j.gastro.2018.01.025.

METHODS: We obtained pancreatic tissues from 5 patients undergoing surgery for pancreatic cancer and prepared 80-μm slices; tissues were exposed to supramaximal cholecystokinin octapeptide (CCK-8) or ethanol and a low concentration of CCK-8 and analyzed by immunoblot and immunofluorescence analyses. STX2-KO mice and *syntaxin* $2^{+/+}$ C57BL6 mice (controls) were given intraperitoneal injections of supramaximal caerulein (a CCK-8 analogue) or fed ethanol and then given a low dose of caerulein to induce acute pancreatitis, or saline (controls); pancreata were isolated and analyzed by histology and immunohistochemistry. Acini were isolated from mice, incubated with CCK-8, and analyzed by immunofluorescence microscopy or used in immunoprecipitation experiments. Exocytosis was quantified using live-cell exocytosis and Ca^{2+} imaging analyses and based on formation of exocytotic soluble N-ethyl maleimide sensitive factor attachment protein receptor complexes. Dysregulations in autophagy were identified using markers, electron and immunofluorescence microscopy, and protease activation assays.

RESULTS: Human pancreatic tissues and dispersed pancreatic acini from control mice exposed to CCK-8 or ethanol plus CCK-8 were depleted of STX2. STX2-KO developed more severe pancreatitis after administration of supramaximal caerulein or a 6-week ethanol diet compared with control. Acini from STX2-KO mice had increased apical exocytosis after exposure to CCK-8, as well as increased basolateral exocytosis, which led to ectopic release of proteases. These increases in apical and basolateral exocytosis required increased formation of fusogenic soluble N-ethyl maleimide sensitive factor attachment protein receptor complexes, mediated by STX3 and STX4. STX2 bound ATG16L1 and prevented it from binding clathrin. Deletion of STX2 from acini increased binding of AT16L1 to clathrin, increasing formation of preautophagosomes and inducing autophagy. Induction of autophagy promoted the CCK-8-induced increase in autolysosome formation and the activation of trypsinogen.

CONCLUSIONS: In studies of human pancreatic tissues and pancreata from STX2-KO and control mice, we found STX2 to block STX3- and STX4-mediated fusion of zymogen granules with the plasma membrane and exocytosis and prevent binding of ATG16L1 to clathrin, which contributes to induction of autophagy. Exposure of pancreatic tissues to CCK-8 or ethanol depletes acinar cells of STX2, increasing basolateral exocytosis and promoting autophagy induction, leading to activation of trypsinogen.

Graphical Abstract

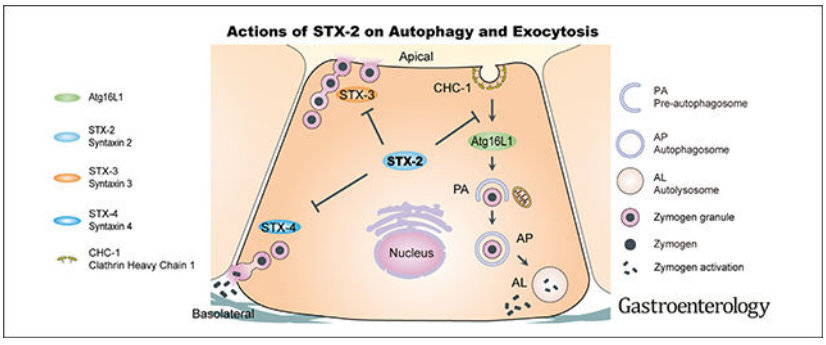

Keywords

SNAREs; Trypsin; Pancreatic Injury; Pathologic Fusion

Pancreatic acinar cells are polarized epithelial cells that store digestive enzymes as inactive zymogens in zymogen granules (ZGs) that are tightly packed into the apical pole.[1] Upon physiologic stimulation by postprandial release of acetylcholine and cholecystokinin octapeptide (CCK-8), acini release enzymes into the gut lumen for food digestion[2] by ZG fusion with the small apical plasma membrane (PM), followed by sequential fusions of ZGs behind apically fused ZGs.[3,4] Exposure to clinically relevant noxious stimuli causing pancreatitis is mimicked by supraphysiologic stimulation (CCK or acetylcholine),[5,6] which triggers 2 initial cellular events of injury.[7] First is formation of large cytoplasmic vacuoles[6,7] caused by an as-yet unclear mechanism in dysregulation of autophagy[8,9] that colocalizes zymogens (trypsinogen) with lysosomal enzymes (cathepsin L/B), whereby activation of both proteases contribute to cell injury.[6,10] Second is ectopic release of zymogens into the interstitial space[11] by blockade of apical exocytosis and redirection of ZGs to fuse with basolateral PM.[12] Both pathologic fusion events lead to premature activation of inactive zymogens, which initiate pancreatitis[8,9,11] that is amplified and/or perpetuated by inflammatory processes.[7,13]

Regulated and pathologic fusion events of pancreatic acini present unique opportunities to test the soluble N-ethyl maleimide sensitive factor attachment protein receptor (SNARE) hypothesis,[14] specifically, how each fusion event is mediated by distinct spatial pairing and assembly of vesicle-SNARE vesicle-associated membrane proteins (VAMPs) and target membrane-SNARE syntaxins and synaptosomal-associated protein of 25 kDa (SNAP25) isoforms into fusion-competent trans-SNARE complexes activated by Sec1/Munc18 (SM) proteins. STX2 on apical PM pairing with ZG-VAMP2[15–17] was initially thought to mediate apical exocytosis. ZG-ZG fusion is mediated by STX3 and VAMP8.[15,18,19] Basolateral exocytosis is mediated by basolateral PM-bound STX4 assembly with VAMP8[19] and SNAP23 (ubiquitous non-neuronal SNAP25),[20] which is activated by Munc18c.[21] The Munc18c/(STX4/VAMP8/SNAP23) complex is activated by clinically relevant toxic ethanol levels (ie, 20 mM ethanol) causing pancreatitis.[19,21,22] Of 4 exocytotic syntaxins, the role of STX2 remains unclear. STX2 was discovered as an epithelial morphogen, called epimorphin,[23] which, when deleted, promoted intestinal epithelial growth.[24] STX2 interactions with VAMP8 played a role in cytokinesis,[25] and interactions with SNAP23-regulated platelet exocytosis.[26]

We show that clinically relevant pancreatitis stimuli,[5,6,19] ethanol, or supraphysiologic CCK-8 stimulation depleted STX2 levels in human pancreatic acini. To elucidate the role of STX2 in pancreatitis, we used STX2-knockout (KO) mice,[24] which showed that STX2 deletion promoted STX4 SNARE complex-mediated basolateral exocytosis. More exciting, STX2 deletion deregulates autophagosome (AP) formation by binding autophagy-related 16-like 1 protein (Atg16L1), which disrupted Atg16L1 interaction with clathrin heavy chain (CHC) required to recruit membranes from PM for physiologic AP formation.[27] These 2 events resulted in increased susceptibility and severity of pancreatitis. Surprising, STX2 does not mediate apical exocytosis per se,[15–17] but rather, STX2 deletion promoted STX3 SNARE complex-mediated apical exocytosis. STX2 has an important role as negative regulator for physiologic and pathologic fusion events in pancreatic acini; the latter poses as a potential therapeutic target for this life-threatening disease that currently has no specific treatment.

Methods

Antibodies and Reagents

Sources of antibodies and reagents are detailed in Supplementary Methods.

Mice, Pancreatitis Induction, Preparation of Tissue Samples, and Histologic Scoring of Acinar Injury

Wild-type (WT) (*syntaxin-2*$^{+/+}$) and STX2-KO (*syntaxin-2*$^{-/-}$, homozygous mutant) mice were obtained from crossing *syntaxin-2*$^{+/-}$ mice (C57BL6).[24] Pancreatitis was induced by 50 μg/kg caerulein administered at 8 hourly intraperitoneal injections; 6-week ethanol (36% of total calorie intake) feeding followed by 5 hourly intraperitoneal low-dose caerulein (0.5 μg/kg) injections. Serum and pancreatic tissues were prepared subsequently for biochemical and histologic studies (described in the Supplementary Material).

Acinar Isolation and Culture, Adenovirus Transduction, HEK293 Cell Culture, and Transfection

Dispersion of pancreatic acini from mice, culture of acinar and HEK cells were reported earlier[28,29] (described in the Supplementary Material).

Human Pancreas Slice Preparation

Portions of human pancreas resected from patients (5 patients; 3 males and 2 females, aged from 60 to 70 years old) with pancreatic cancer were obtained from the Surgical Pathology Laboratory of the Toronto General Hospital. Pancreas tissue slices (80-μm-thick) were prepared as reported recently[30] (described in the Supplementary Material).

Imaging of Intracellular Ca^{2+} and Exocytosis, Confocal, and Electron Microscopy

Intracellular calcium ($[Ca^{2+}]_i$ was tracked with Fura-2 AM using epifluorescence microscopy.[31] Spinning disk confocal microscope was employed for exocytosis imaging of dispersed acini treated with FM1–43 dye or infected with adenovirus-syncollin-pHluorin, and also for immunofluorescence experiments. Electron microscopy was performed for ultrastructural studies as reported previously.[19,22] See the Supplementary Material.

Immunoprecipitation, Enzyme Assays, and Subcellular Fractionation

These were performed essentially as described earlier[22,32,33] (see Supplementary Methods).

Densitometric and Morphometric Analyses

ImageJ (ImageJ; National Institutes of Health; http://rsb.info.nih.gov/ij) was used to quantify intensities of bands obtained in Western blots and RT-PCR. Radiuses of ZGs were measured after scale adjustment.[28]

Statistics

Statistical analyses were performed by one-way analysis of variance using ORIGIN (Microcal, Amherst, MA) or 2-tailed Student *t* test using Excel (Microsoft, Redmond, WA). Data are presented as means ± SEM. A *P* value <.05 was considered statistically significant.

Study Approval

Animal procedures and use of human pancreas were performed in accordance with the University of Toronto's Animal Care Committee's ethical guidelines and Research Ethics Board of the University Health Network of Toronto.

Results

Pancreatitis Stimuli of Human Pancreas Depletes STX2 Levels Inducing Autophagic Vacuole Formation

We used well-established pancreatitis stimuli that simulate human pancreatitis, including supraphysiologic CCK stimulation (100 nM, 2 hours) and 20 mM ethanol (EtOH) preincubation (1 hour) followed by physiologic CCK (100 pM, 2 hours) stimulation,[5,6,12,19] to treat human pancreas slices (similar levels of mTOR, ERK1/2, and light-chain 3B (LC3B) I/II as mouse pancreas in Supplementary Figure 1A) obtained from surgical resections for pancreatic cancer[30] (Figure 1) and mouse acini (Supplementary Figure 1B). We assessed the effects on SNARE fusion machineries,[34] which showed severe reduction in STX2 levels in the human pancreatic slices (100 nM CCK: 77%; 20 mM EtOH + 100 pM CCK: 84%) and mouse acini (100 nM CCK: 69%; CCK + EtOH: 74%) without affecting other SNARE proteins (Supplementary Figure 1C and 1D). As expected, these pancreatitis treatments caused an increase in levels of phosphatidylethanolamine-conjugated microtubule-associated protein-1 LC3B-II relative to LC3B-I (human: 100 nM CCK: 400%; EtOH + CCK: 430%; mouse: 100 nM CCK: 370%; EtOH + CCK: 389%; and accumulation of LC3B-positive autophagic vacuole (AVs) (Figure 1B).[8,9,30,35] We recently reported that supraphysiologic CCK or cholinergic stimulation of human pancreatic slices induced basolateral exocytosis and apical blockade along with protease activation,[30] as similarly observed in rodent pancreatic acini.[6,7,12,19]

STX2, normally enriched in apical PM lining the pancreatic ductal lumen where actin is abundant (Figure 1B, control), was completely disrupted by the pancreatitis treatments (Figure 1B, 100 nM CCK or EtOH + CCK), with residual degraded cytosolic STX2 situated along the basolateral pole adjacent to the basolateral PM, marked by weaker actin abundance. We found that cysteine protease inhibitor E64d could fully restore the full-length STX2, whereas the proteasome inhibitor MG132 prevented the large STX2 cleavage product from further degradation (Figure 1C). The pancreatitis treatments did not affect the expression or basolateral PM localization of STX4 (Supplementary Figure 1F). Because SNARE proteins were shown to influence autophagy,[36,37] we postulated that STX2 has a new role in autophagy in addition to exocytosis, which we explored using a global STX2-KO mouse.

STX2 Deletion Paradoxically Augments CCK-Stimulated Amylase Secretion

We verified the expression of STX2 and other exocytotic proteins in WT and STX2-KO pancreatic acini. Of 4 STX2 variants: STX2A/2B(32 kDa), 2C(29 kDa), 2D(26 kDa), mouse acini express only STX2A/2B with larger abundance (approximately 80%) of STX2A (Supplementary Figure 2A and 2B). STX2 was absent (Figure 2A) in STX2-KO acini,[24] whereas levels of STXs (−3, −4), VAMPs (−2, −8), SNAP23, and SM proteins (Munc18b,c)

were unaffected (Supplementary Figure 2C and 2D). STX2 deletion was confirmed by its absence in the apical PM, where it normally co-localizes with actin (Supplementary Figure 2E).[15,17] STX2-KO did not affect morphology, wherein STX2-KO acini remained fully polarized.

CCK-8 stimulates amylase secretion in a biphasic manner,[2] with a physiologic dose-dependent to a peak response (10–100 pM), followed by progressive reduction from maximal levels at supraphysiologic doses (>1000 pM to 20 nM). The latter is due to blockade in apical exocytosis and redirection of ZGs to fuse with basolateral PM,[12] which contributes to pancreatitis.[7] Because STX2 was postulated to act as a pro-fusion SNARE,[17] its deletion should reduce secretion. Surprisingly, STX2 deletion resulted in paradoxical enhancement of amylase secretion (Figure 2B) at submaximal CCK (10–20 pM), but to a similar maximal peak response (100 pM). At supramaximal CCK (1–20 nM), this enhancement of secretion persisted in STX2-KO acini. Total amylase content of STX2-KO acini was similar to WT acini (Figure 2C). STX2/GFP overexpression (approximately 2.2-fold) into STX2-KO acini (Figure 6D) restored (reduced) the submaximal and supramaximal secretory responses, mimicking Ad-GFP-transduced WT acini (Figure 2D). Because Ca^{2+} is the primary fusogenic signal for ZG exocytosis,[38] we assessed the intracellular Ca^{2+} responses (Supplementary Figures 2F-2H) at basal, submaximal 10 pM (oscillatory responses) and supramaximal 10 nM CCK-8 stimulation (high peak decreasing to a low plateau responses), which were not different between WT and STX2-KO acini. These results suggest that enhancement of secretion in STX2-KO acini is likely at an exocytotic step downstream from Ca^{2+} release.

STX2 Deletion Augments Physiologic CCK-Stimulated Apical Exocytosis and Supraphysiologic CCK-Stimulated Basolateral Plasma Membrane Exocytosis

Lipophilic dye FM1–43 fluoresces on contact with lipid PM, appearing as hotspots on PM when it permeates into ZGs undergoing exocytosis.[12,21,22,39] We selected 4- to 7-cell acini for optimal microscopic visualization. In WT acini (Figure 3Ai), there were no hotspots at basal state. On 10 pM CCK-8 stimulation, we saw time-dependent moderate but progressive increase in fluorescent area and intensity, indicating ZG exocytosis (ZG-apical PM fusion and sequential ZG-ZG fusions) at the apical region of the acinus (*arrows*), with no exocytosis occurring in the basolateral PM. In STX2-KO acini, 10 pM CCK-8 caused larger and higher fluorescence intensity increase at the apical pole (graphical analysis, Figure 3Aii). The 10 nM CCK-8 stimulation blocked apical exocytosis (*arrows*) and redirected exocytosis to basolateral PM (*arrowheads*)[12,19] (Figure 3Bi). STX2-KO caused an exaggerated exocytotic response at the basal PM (*arrowheads*). Remarkably, STX2-KO restored apical exocytosis (*arrows*). Both exaggerated exocytotic responses caused by STX2 deletion are depicted in graphical analysis (Figure 3Bii).

FM1–43 has disadvantages of persistent FM1–43 fluorescence when endocytosed and may not readily permeate into ZGs fusing with the less accessible lateral PM, which may explain why exocytosis was largely limited to the junctions of basal and lateral PM (Figure 3Bi). We tracked ZG exocytosis at high spatiotemporal resolution by infecting acini with Ad-syncollin-pHluorin[22] (Figure 3C and 3D). Syncollin, an endogenous ZG content protein,

when fused to pH-dependent GFP pHluorin, instantaneously fluoresces in alkaline pH upon exposure of exocytosing ZGs to the cell exterior, and enables tracking of sequential fusion of deeper layers of ZGs. Closure of fusion pores results in ZG reacidification, which reduces fluorescence, providing excellent signal-to-noise recording. The 10 pM CCK-8-stimulated exocytosis at apical PM of WT acini (Figure 3Ci) was amplified by 2.5× in STX2-KO acini, with far more sequential fusions with deeper layers of ZGs. There were very few fusions at the basal or lateral PM. Detailed analysis of total fusion events (Figure 3Cii, normalized to cell area and recording time) showed much-enhanced apical exocytosis in STX2-KO acini, which accounted for almost all of total acinar exocytosis, with very little contribution from basolateral exocytosis. With 10 nM CCK-8 stimulation, WT acini showed a hazy low-level fluorescence at the apical region but no exocytotic hotspots (Figure 3Di), and some bright hotspots occurring at the basal and lateral PM (*arrowheads*). In STX2-KO acini, 10 nM CCK-8 stimulated more basolateral exocytosis (*arrowheads*), some appearing as compound and sequential fusions (compare second and third images). Of note, 10 nM CCK-8 stimulated abundant apical exocytosis, mimicking 10 pM CCK-8 stimulation (Figure 3Ci). More detailed analysis (Figure 3Dii) showed 2.7× enhancement of total exocytosis in 10 nM CCK-8-stimulated STX2-KO acini, which was contributed more from enhanced basolateral exocytosis and less from relief of apical exocytotic blockade. Figure 3Ci and Di are shown in larger images in Supplementary Figure 3A and 3B, respectively, and in real-time in Movies 1–4.

STX2 Deletion Promotes Assembly of Apical (STX3) and Basolateral (STX4) SNARE Complexes

We assessed for distinct SM-SNARE complexes, which could account for these changes in exocytosis caused by STX2 deletion. Previous reports suggested that Munc18b/(STX3/SNAP23) complex with ZG-SNARE VAMP8 mediates physiologic CCK-stimulated exocytosis at apical PM and subsequent sequential ZG-ZG fusion[18,19]; while Munc18c/(STX4/SNAP23/VAMP8) complex mediates supramaximal CCK-induced basolateral exocytosis.[12,19] Co-immunoprecipitation studies with STX3 (Figure 4A) and STX4 (Figure 4B) antibodies confirmed these SM/SNARE complexes in WT acini. Munc18b/(STX3/SNAP23/VAMP8 (VAMP2 to lesser extent) complexes were more abundant in STX2-KO acini (Figure 4A) at comparable physiologic CCK-8 (10 pM, 100 pM) stimulation, consistent with the increased apical exocytosis (Figure 3A and 3C). At supramaximal (10 nM) CCK-8 stimulation of STX2-KO acini, formation of apical SM/SNARE complexes was, remarkably, as abundant as 100-pM CCK-8 stimulation, consistent with the intact apical exocytosis (Figure 3B and 3D). This is in contrast to the reduced amounts of this SM/SNARE complex in 10 nM CCK stimulation of WT acini, consistent with the blocked apical exocytosis (Figure 3B and 3D). Basolateral Munc18c/(STX4/SNAP23/VAMP8) complex seen only at 10 nM CCK-8 stimulation of WT acini (Figure 4B), was more abundant in STX2-KO acini, and observed at lower CCK-8 doses, consistent with the larger basolateral exocytotic responses (Figure 3B and 3D). The changes in Munc18b and Munc18c levels[12] within these SM/SNARE complexes are explained in Supplementary Figure 4. Using co-expression in HEK cells and co-immunoprecipitation, the above can be at least partly explained by the ability of STX to compete with STX3 and STX4 from forming cognate complexes with VAMP8 and VAMP2 (Figure 4C). This is consistent with STX2 reported

recently to possibly act as i-SNARE in pancreatic β cells, whereby STX2 deletion promoted formation of STX1A- and STX3 SNARE complexes, which amplified insulin granule exocytosis.[40]

STX2 Deletion Increases Autophagosome Formation by Enhancing Atg16L1/CHC Complex Assembly, Which Amplifies CCK Hyperstimulation-Induced Impairment in Autolysosome Clearance

Increased accumulation of AVs along with depletion of STX2 in human pancreas exposed to pancreatitis treatments (Figure 1) led us to investigate their causative link using the STX2-KO pancreas. Similar to the human pancreas results (Figure 1), STX2-KO acini showed more LC3B-GFP punctae, with a 109% increase in control condition and a further 85% increase after 10 nM CCK stimulation (Supplementary Figure 5Ai and 5Aii). Consistently, STX2-KO acini showed more elevated LC3B-II conversion (83.5%) under control condition (no CCK-8), becoming further increased by 10 nM CCK-8 stimulation (LC3B-II: 179%, Supplementary Figure 5Bi). In the presence or absence of saturating concentrations of lysosome degradation inhibitor bafilomycin,[41,42] LC3B-II levels increased in STX2-KO acini without or with CCK-8 hyperstimulation (Supplementary Figure 5Bii). STX2 deletion therefore increases AV accumulation and autophagy induction.[41,42]

Supramaximal caerulein (frog CCK decapeptide functionally equivalent to CCK-8)[5,6]-induced AV accumulation in acini was reported to be caused by induced defects in lysosomal clearance[9] resulting in accumulation of early autolysosomes. CCK-8 (10 nM)-stimulated STX2-KO acini displayed consistent increase in LC3B-GFP punctae and accumulation of LC3B-GFP punctae within LAMP-2-positive vacuoles much more than WT acini (Supplementary Figure 5Ci). This indicates increased formation of APs (LC3B-GFP-positive) and early autolysosomes (LC3B-GFP/LAMP-2-positive) in STX2-KO acini. Using transmission electron microscopy (Figure 5Ai), we assessed these morphologically distinct cellular structures (Supplementary Figure 5D; AP: double membrane with undigested content; early autolysosome (EAL): single membrane with undigested content and late autolysosome: single membrane with amorphous electron-dense content); qualitatively and quantitatively (Figure 5Aii) to track how STX2 deletion perturbed AV maturation. In STX2-KO acini, AVs were higher by 103% in control and 122% after CCK stimulation (Figure 5Aii, *top*). In control (no CCK) acini (Figure 5Aii, *bottom*), STX2 deletion caused an 85% increase in APs, but no significant changes in EAL (21% increase) and late autolysosome (11% increase), indicating induction of autophagy. With supramaximal CCK stimulation, STX2-KO compared to WT acini caused a further 66% increase in AP formation and 63% increase in EALs, and insignificant 2% increase in late autolysosomes, indicating impairment in the autophagic flux. Analysis of lysosomal cathepsins (Supplementary Figure 5Ei, cathepsin L (*left*) and B (*right*) activity; Supplementary Figure 5Eii shows lysosome fractionation purity) revealed the expected impairment in cathepsin activation resulting from supramaximal CCK-8 stimulation postulated to explain the observed defect in AL degradation[9]; this was, however, not altered by STX2 deletion. Supplementary Figure 5F shows similar number and size of ZGs between WT and STX2-KO acini. As total amylase content was also similar between WT and STX2-KO acini (Figure 2C), this indicates that

STX2 deletion does not affect ZG maturation or synthesis of ZG proteases to explain these results.

The enhanced formation of AVs in STX2-KO acini could be due to effects on fusion events underlying AP biogenesis. Whereas other SNARE proteins have been shown to influence fusion events occurring during autophagy,[37,43] we could not detect the presence of STX2 in APs, endosomes, or lysosomes by immunofluorescence or by subcellular fractions in control (data not shown) and supraphysiological CCK-stimulated acini (Supplementary Figure 5G). Interestingly, in HeLa cells, Atg16L1 was shown to translocate to PM during intense autophagy to gain more membranes for AP biogenesis, which is mediated by PM-bound CHC-1 forming a complex with pre-AP–linked Atg16L1.[27] We examined the possibility that PM-bound STX2 could influence CHC1-Atg16L1 complex assembly. Immunoprecipitation of Atg16L1 (Figure 5Bi) pulled down more CHC-1 in STX2-KO than WT acini at basal (by 122.5%) and after 10 nM CCK-8 stimulation (by 49%). This would suggest that STX2-KO increased CHC-1 incorporation into Atg16L1 vesicles (Figure 5Bii and 5Biii). In unstimulated acini, CHC-1 vesicles were similarly few between WT and STX2-KO acini (WT: 1.87 ± 0.24, STX2-KO: 2.1 ± 0.31), although Atg16L1 vesicles were higher in STX2-KO acini (WT: 2.39 ± 0.48, STX2-KO: 4.47 ± 0.66). The 10 nM CCK-8 stimulation increased the number of CHC-1 vesicles much more in STX2-KO acini (WT: 2.64 ± 0.43, 48%; STX2-KO: 6.29 ± 0.68, 200%); likewise there were more Atg16L1 vesicles in STX2-KO acini (WT: 5.76 ± 1.11, 42%; STX2-KO: 12.39 ± 1.81, 277%). Colocalized CHC-1/Atg16L1 vesicles were 1.5× higher in control STX2-KO acini (WT: 1.21 ± 0.16, STX2-KO: 1.97 ± 0.28), which further increased 3× (WT: 2.19 ± 0.33, STX2-KO: 6.29 ± 0.78) after 10 nM CCK-8 stimulation. This suggests an increased contribution of PM to pre-AP formation in STX2-KO acini.

Increased pre-AP formation is expected to feed phagophore elongation and closure, forming more and larger APs,[42,44] which is assessed by the extent of Atg16L1 incorporation into LC3 vesicles (Figure 5C). As mentioned, Atg16L1 vesicles were more in STX2-KO acini in control and after 10 nM CCK-8 stimulation. There were more Atg16L1/LC3 colocalized vesicles in STX2-KO acini (WT: 3.69 ± 0.66, STX2-KO: 9.27 ± 1.1), which also had higher mean vesicle volumes (unstimulated, WT: 0.921 ± 0.072 μm^2/STX2-KO: 1.44 ± 0.112 μm^2; stimulated, WT: 1.086 ± 0. 083 μm^2/STX2-KO: 1.53 ± 0.14 μm^2).

Furthermore, Atg16L1 pulldown co-immunoprecipitated STX2 from WT acini at basal state, which increased by 112% after 10 nM CCK-8 stimulation (Figure 5Di). To confirm, a reciprocal study of STX2 pulldown (Figure 5Dii) immunoprecipitated both Atg16L1 and CHC-1, which increased by 44% and 34%, respectively, after 10 nM CCK-8 stimulation. Increases in Atg5–12 binding to Atg16L1 (Figure 5Di) and SNAP23 binding to STX2 (Figure 5Dii) were used as positive controls. To assess which protein within the Atg16L1-CHC complex STX2 actually binds to, in HEK cells co-expressing FLAG-Atg16L1 (Figure 5E) or GFP-CHC-1 (Figure 5F) with STX2, STX2 and Atg16L1 reciprocally immunoprecipitated each other, but there was no binding between CHC-1 and STX2. STX2 dose-dependently competed off CHC-1 binding to Atg16L1 (Figure 5G). This suggests that STX2 negatively regulates Atg16L1 assembly with CHC-1 by physically interacting with

Atg16L1 to sequester it from CHC-1. We conclude that STX2 deletion in acini acts to enhance Atg16L1/CHC-1 assembly, which in turn promotes autophagy.[27]

STX2 Deletion Promotes Autolysosomal Trypsinogen Activation

Intra-acinar premature trypsinogen activation, a key event causing pancreatitis,[6,13,45] occurs primarily in cytoplasmic vacuoles,[6,46] which were recently linked to perturbed autophagy[8] and identified to occur in early autolysosomes (LC3B/LAMP-2–positive vacuoles).[9] Because STX2-KO acini accumulated more EALs, we assessed whether EAL is the cellular location of trypsin- ogen activation using the marker trypsinogen activation peptide (TAP) against LC3B-GFP-positive (AVs) and LAMP-2-positive vacuoles (lysosomes). STX2-KO acini showed more AVs (LC3B-GFP puncta) at both basal (Figure 6Ai, *top panel*) and 10 nM CCK stimulation (Figure 6Ai, *bottom panel*). Trypsinogen activation (TAP) occurred predominantly within these AVs (Figure 6Ai) and lysosomes (Figure 6Bi) after CCK-8 stimulation. In STX2-KO acini stimulated with 10 nM CCK, there was an 83% increase in LC3B/TAP-positive vacuoles (Figure 6Aii) and 59% increase in LAMP2/TAP-positive vacuoles (Figure 6Bii), consistent with higher intracellular trypsin activity (69% increase) (Figure 6C). We did not observe any significant difference in trypsin activity in control (no CCK) cells where autophagy remained functional. To unequivocally show that excessive AV formation and intracellular trypsinogen activation were functional consequences of STX2 deletion, we performed STX2 rescue expression. STX2/GFP overexpression (approximately 2.2-fold) into STX2-KO acini reduced LC3B-I to LC3-BII conversion (Figure 6D, also in control acini) and also reduced intracellular trypsinogen activation (Figure 6E) to levels similar to Ad-GFP-transduced WT acini after 10 nM CCK-8 stimulation.

STX2 Deletion Increases Susceptibility to Caerulein- and Ethanol-Induced Pancreatitis

An increase in basolateral exocytosis (Figures 3 and 4) and autolysosomal protease activation (Figure 6) in STX2-KO acini would predict increased susceptibility to pancreatitis, which we tested employing two mild pancreatitis protocols: supramaximal caerulein (Figure 7A) and ethanol-fed pancreatitis (6-week ethanol diet followed by low-dose caerulein, Figure 7B).[5,6,19,33] Pancreatic injury was assessed by scoring (1–4) 4 histologic parameters individually (Figure 7Ai and 7Bii, *top*) and as total histology scores (Figure 7Aii and 7Bii; *bottom*). In saline control, only vacuolization was higher in STX2-KO pancreas, which did not affect the total histology score or pancreatic trypsinogen activation (Figure 7Aiii and 7Biii). However, with both supramaximal caerulein- and ethanol-fed pancreatitis models, STX2-KO pancreas showed more edema, inflammation, vacuolization, and necrosis (Figure 7Aii and 7Bii). A larger increase in trypsin activity was observed in STX2-KO pancreas in both models (Figure 7Aiii and 7Biii). We confirmed that both caerulein- and ethanol diet-induced pancreatic inflammation were attributed to polymorphonuclear leukocyte infiltration by myeloperoxidase assay (Figure 7Aiii and 7Biii), which were higher in the STX2-KO pancreas. Finally, we measured clinically used pancreatitis parameters of circulating pancreatic enzymes amylase and lipase (Figure 7Aiv and 7Biv), which were also higher in STX2-KO mice for both pancreatitis models. These results collectively indicate that STX2 deletion in mice, mimicking STX2 depletion by the pancreatitis stimuli of human pancreas (Figure 1), is mechanistically linked to increased susceptibility and severity of pancreatitis.

Discussion

STX2-KO up-regulated supraphysiologic CCK-mediated pathologic basolateral exocytosis and the formation of AVs, both with consequent protease activation, which enhanced pancreatitis. STX2, therefore, presents a unique common target to abrogate these 2 central early events that underlie pancreatitis.[6,9,11] STX2-KO also up-regulated physiologic CCK-8-stimulated apical exocytosis. VAMP8 was recently reported to also influence both secretion and autophagy.[47] While therapeutically enhancing STX2 actions could reduce physiologic release of pancreatic enzymes, only a small fraction of pancreatic enzymes is actually needed for effective food digestion[48]; and such likely clinically inconsequential deficiency could be easily replaced by exogenous enzyme treatment.[49]

Our results show that STX2 negatively regulates 3 disparate fusion events (see graphical abstract). First, STX2 competes with STX3 from forming STX3/SNAP23/VAMP8 (and VAMP2) complexes required for apical exocytosis.[18,19,22] Second, STX2 competes with STX4 from forming STX4/SNAP23/VAMP8 complexes that mediate basolateral exocytosis.[12,19,22] In both, STX2 seems to functionally act as an inhibitory SNARE (i-SNARE), forming non-fusogenic complexes, as we reported in β-cells.[40] This concept of i-SNAREs, shown first by in vitro lipid fusion, was postulated to provide a mechanism for countercurrent fusion occurring in Golgi stacks.[50] Physiologically, i-SNAREs' apparent deliberate mechanism to reduce efficiency of membrane fusion adds to the plasticity of secretory cells like acini to effect a slower secretory rate (than neurons) of digestive enzyme release over hours to ensure optimal nutrient digestion after a meal, which matches the slow processes of nutrient absorption and assimilation. It is possible that STX2 might not be a pure i-SNARE per se, but rather acts as an inefficient fusion protein that competes with fusion-competent syntaxins. Third, STX2 binds Atg16L1, which is not a SNARE protein, to block its assembly with CHC, which mediates pre-AP formation.[27] AP fusion processes employ a very different set of proteins forming distinct complexes,[44] which we have only begun to examine in pancreatic acini, and are influenced by "anti-fusion" STX2 (this report) and other "pro-fusion" SNARE proteins (eg, VAMP7, STX7, and STX8) reported to be involved in autophagy.[37,43] STX2 regulation of Atg16L1 likely plays a broader role in autophagy in other gastrointestinal tissues, such as in intestinal epithelial cells in the defense against invasive bacterial pathogens,[51] and in the pathogenesis of inflammatory bowel diseases.[52]

Supplementary Material

Refer to Web version on PubMed Central for supplementary material.

Acknowledgments

The authors thank Junichi Sadoshima (Rutgers New Jersey Medical School, Rutherford, NJ) for LC3B-GFP adenovirus; Dana Philpott (University of Toronto, Toronto, ON, Canada) for pLJM1-FLAG-ATG16L1; Stephen Royle (Warwick Medical School, Coventry, UK) for pBrain-GFP-CHC(1–1675). Fei Kang for artwork. The authors thank the patients, surgeons, pathologists, and staff of University Health Network Program in Biospecimen Sciences for providing the normal pancreatic tissues.

Funding

This work was supported by a grant from Canadian Institute of Health Research (CIHR, MOP 119352) to H.Y.G. S.D. is funded by a postdoctoral fellowship from Canadian Association of Gastroenterology and CIHR (CAG-CIHR). Some of the equipment used in this study was supported by the 3D (Diet, Digestive Tract and Disease) Centre funded by the Canadian Foundation for Innovation and Ontario Research Fund, project number 19442.

Abbreviations used in this paper:

AP	autophagosome
Atg16L1	autophagy-related 16-like 1 protein
AV	autophagic vacuoles
CCK-8	cholecystokinin octapeptide
CHC	clathrin heavy chain
AL	autolysosome
EAL	early autolysosome
i-SNARE	inhibitory soluble N-ethyl maleimide sensitive factor attachment protein receptor
KO	knockout
LC3B	light-chain 3B
PM	plasma membrane
SM	Sec1/Munc18
SNAP23	synaptosomal-associated protein of 23 kDa
SNAP25	synaptosomal-associated protein of 25 kDa
SNARE	soluble N-ethyl maleimide sensitive factor attachment protein receptor
TAP	trypsinogen activation peptide
VAMP	vesicle-associated membrane protein
WT	wild-type
ZG	zymogen granule

References

1. Palade G Intracellular aspects of the process of protein synthesis. Science 1975;189:867. [PubMed: 17812524]
2. Williams JA. Stimulus-Secretion Coupling In Pancreatic Acinar Cells. New York: Raven Press, 1993.
3. Dolai S, Liang T, Cosen-Binker LI, Lam PPL, Gaisano HY. Regulation of physiologic and pathologic exocytoses in pancreatic acinar cells. The Pancreapedia: Exocrine Pancreas Knowledge

Base. Available at: https://www.pancreapedia.org/reviews/regulation-of-physiologic-and-pathologic-exocytosis-in-pancreatic-acinar-cells. Accessed March 12, 2018.

4. Nemoto T, Kimura R, Ito K, et al. Sequential-replenishment mechanism of exocytosis in pancreatic acini. Nat Cell Biol 2001;3:253–258. [PubMed: 11231574]
5. Lerch MM, Gorelick FS. Models of acute and chronic pancreatitis. Gastroenterology 2013;144:1180–1193. [PubMed: 23622127]
6. Steer ML, Meldolesi J. The cell biology of experimental pancreatitis. N Engl J Med 1987;316:144–150. [PubMed: 3540666]
7. Gaisano HY, Gorelick FS. New insights into the mechanisms of pancreatitis. Gastroenterology 2009; 136:2040–2044. [PubMed: 19379751]
8. Hashimoto D, Ohmuraya M, Hirota M, et al. Involvement of autophagy in trypsinogen activation within the pancreatic acinar cells. J Cell Biol 2008; 181:1065–1072. [PubMed: 18591426]
9. Mareninova OA, Hermann K, French SW, et al. Impaired autophagic flux mediates acinar cell vacuole formation and trypsinogen activation in rodent models of acute pancreatitis. J Clin Invest 2009;119:3340–3355. [PubMed: 19805911]
10. Talukdar R, Sareen A, Zhu H, et al. Release of cathepsin B in cytosol causes cell death in acute pancreatitis. Gastroenterology 2016;15:747–758.
11. Hartwig W, Jimenez RE, Werner J, et al. Interstitial trypsinogen release and its relevance to the transformation of mild into necrotizing pancreatitis in rats. Gastroenterology 1999;117:717–725. [PubMed: 10464149]
12. Gaisano HY, Lutz MP, Leser J, et al. Supramaximal cholecystokinin displaces Munc18c from the pancreatic acinar basal surface, redirecting apical exocytosis to the basal membrane. J Clin Invest 2001;108:1597–15611. [PubMed: 11733555]
13. Sah RP, Garg P, Saluja AK. Pathogenic mechanisms of acute pancreatitis. Curr Opin Gastroenterol 2012; 28:507–515. [PubMed: 22885948]
14. Sudhof TC, Rothman JE. Membrane fusion: grappling with SNARE and SM proteins. Science 2009;323: 474–477. [PubMed: 19164740]
15. Gaisano HY, Ghai M, Malkus PN, et al. Distinct cellular locations of the syntaxin family of proteins in rat pancreatic acinar cells. Mol Biol Cell 1996;7:2019–2027. [PubMed: 8970162]
16. Gaisano HY, Sheu L, Foskett JK, et al. Tetanus toxin light chain cleaves a vesicle-associated membrane protein(VAMP) isoform-2 in rat pancreatic zymogen granules and inhibits enzyme secretion. J Biol Chem 1994; 269:17062–17066. [PubMed: 7516331]
17. Pickett JA, Thorn P, Edwardson JM. The plasma membrane Q-SNARE syntaxin-2 enters the zymogen granule membrane during exocytosis in the pancreatic acinar cell. J Biol Chem 2005;280:1506–1511. [PubMed: 15536072]
18. Behrendorff N, Dolai S, Hong W, et al. Vesicle-associated membrane protein-8(VAMP8) is a SNARE (soluble N-ethylmaleimide-sensitive factor attachment protein receptor) selectively required for sequential granule-to-granule fusion. J Biol Chem 2011;286:29627–29634. [PubMed: 21733851]
19. Cosen-Binker LI, Binker MG, Wang CC, et al. VAMP8 is the v-SNARE that mediates basolateral exocytosis in a mouse model of alcoholic pancreatitis. J Clin Invest 2008;118:2535–2551. [PubMed: 18535671]
20. Huang X, Sheu L, Tamori Y, et al. Cholecystokinin-regulated exocytosis in rat pancreatic acinar cells is inhibited by a C-terminus truncated mutant of SNAP-23. Pancreas 2001;23:125–133. [PubMed: 11484914]
21. Cosen-Binker LI, Lam PP, Binker MG, et al. Alcohol/ cholecystokinin-evoked pancreatic acinar basolateral exocytosis is mediated by protein kinase C alpha phosphorylation of Munc18c. J Biol Chem 2007; 282:13047–13058. [PubMed: 17324928]
22. Dolai S, Liang T, Lam PP, et al. Effects of ethanol metabolites on exocytosis of pancreatic acinar cells in rats. Gastroenterology 2012;143:832–843. [PubMed: 22710192]
23. Hirai Y, Takebe K, Takashina M, et al. Epimorphin: a mesenchymal protein essential for epithelial morphogenesis. Cell 1992;69:471–481. [PubMed: 1581962]

24. Wang Y, Wang L, Iordanov H, et al. Epimorphin(−/−) mice have increased intestinal growth, decreased susceptibility to dextran sodium sulfate colitis, and impaired spermatogenesis. J Clin Invest 2006;116: 1535–1546. [PubMed: 16710473]
25. Low SH, Li X, Miura M, et al. Syntaxin-2 and endobrevin are required for the terminal step of cytokinesis in mammalian cells. Dev Cell 2003;4:753–759. [PubMed: 12737809]
26. Chen D, Bernstein AM, Lemons PP, et al. Molecular mechanisms of platelet exocytosis: role of SNAP-23 and syntaxin-2 in dense core granule release. Blood 2000; 95:921–929. [PubMed: 10648404]
27. Ravikumar B, Moreau K, Jahreiss L, et al. Plasma membrane contributes to the formation of preautophagosomal structures. Nat Cell Biol 2010;12: 747–757. [PubMed: 20639872]
28. Dolai S, Xie L, Zhu D, et al. Synaptotagmin-7 functions to replenish insulin granules for exocytosis in human islet beta-cells. Diabetes 2016;65:1962–1976. [PubMed: 27207520]
29. Fernandez NA, Liang T, Gaisano HY. Live pancreatic acinar imaging of exocytosis using syncollin-pHluorin. Am J Physiol Cell Physiol 2011;300:C1513–C1523. [PubMed: 21307342]
30. Liang T, Dolai S, Xie L, et al. Ex vivo human pancreatic slice preparations offer a valuable model for studying pancreatic exocrine biology. J Biol Chem 2017; 292:5957–5969. [PubMed: 28242761]
31. Thorn P, Lawrie AM, Smith PM, et al. Local and global cytosolic Ca2+ oscillations in exocrine cells evoked by agonists and inositol trisphosphate. Cell 1993;74: 661–668. [PubMed: 8395347]
32. Meldolesi J, Jamieson JD, Palade GE. Composition of cellular membranes in the pancreas of the guinea pig. I. Isolation of membrane fractions. J Cell Biol 1971;49: 109–129. [PubMed: 4324564]
33. Saluja A, Saito I, Saluja M, et al. In vivo rat pancreatic acinar cell function during supramaximal stimulation with caerulein. Am J Physiol 1985;249:G702–G710. [PubMed: 2417493]
34. Jahn R, Scheller RH. SNAREs—engines for membrane fusion. Nat Rev Mol Cell Biol 2006;7:631–643. [PubMed: 16912714]
35. Pandol SJ, Lugea A, Mareninova OA, et al. Investigating the pathobiology of alcoholic pancreatitis. Alcohol Clin Exp Res 2011;35:830–837. [PubMed: 21284675]
36. Moreau K, Renna M, Rubinsztein DC. Connections between SNAREs and autophagy. Trends Biochem Sci 2013;38:57–63. [PubMed: 23306003]
37. Nair U, Jotwani A, Geng J, et al. SNARE proteins are required for macroautophagy. Cell 2011;146:290–302. [PubMed: 21784249]
38. Petersen OH, Tepikin AV. Polarized calcium signaling in exocrine gland cells. Annu Rev Physiol 2008;70:273–299. [PubMed: 17850212]
39. Lam PP, Cosen Binker LI, Lugea A, et al. Alcohol redirects CCK-mediated apical exocytosis to the acinar basolateral membrane in alcoholic pancreatitis. Traffic 2007;8:605–617. [PubMed: 17451559]
40. Zhu D, Xie L, Kang Y, Dolai S, et al. Syntaxin-2 acts as inhibitory SNARE for insulin granule exocytosis. Diabetes 2017;66:948–959. [PubMed: 28115395]
41. Mizushima N, Yoshimori T, Levine B. Methods in mammalian autophagy research. Cell 2010;140: 313–3126. [PubMed: 20144757]
42. Klionsky DJ, Abdalla FC, Abeliovich H, et al. Guidelines for the use and interpretation of assays for monitoring autophagy. Autophagy 2012;8:445–544. [PubMed: 22966490]
43. Moreau K, Ravikumar B, Renna M, et al. Autophagosome precursor maturation requires homotypic fusion. Cell 2011;146:303–317. [PubMed: 21784250]
44. Xie Z, Klionsky DJ. Autophagosome formation: core machinery and adaptations. Nat Cell Biol 2007;9: 1102–1109. [PubMed: 17909521]
45. Gaiser S, Daniluk J, Liu Y, et al. Intracellular activation of trypsinogen in transgenic mice induces acute but not chronic pancreatitis. Gut 2011;60:1379–1388. [PubMed: 21471572]
46. Sherwood MW, Prior IA, Voronina SG, et al. Activation of trypsinogen in large endocytic vacuoles of pancreatic acinar cells. Proc Natl Acad Sci U S A 2007;104: 5674–5679. [PubMed: 17363470]
47. Messenger SW, Jones EK, Holthaus CL, et al. Acute acinar pancreatitis blocks vesicle-associated membrane protein-8(VAMP8)-dependent secretion, resulting in intracellular trypsin accumulation. J Biol Chem 2017; 292:7828–7839. [PubMed: 28242757]

48. DiMagno EP, Go VL, Summerskill WH. Relations between pancreatic enzyme ouputs and malabsorption in severe pancreatic insufficiency. N Engl J Med 1973; 288:813–815. [PubMed: 4693931]

49. DiMagno EP, Malagelada JR, Go VL, et al. Fate of orally ingested enzymes in pancreatic insufficiency. Comparison of two dosage schedules. N Engl J Med 1977; 296:1318–1322. [PubMed: 16213]

50. Varlamov O, Volchuk A, Rahimian V, et al. i-SNAREs: inhibitory SNAREs that fine-tune the specificity of membrane fusion. J Cell Biol 2004;164:79–88. [PubMed: 14699088]

51. Travassos LH, Carneiro LA, Ramjeet M, et al. Nod1 and Nod2 direct autophagy by recruiting ATG16L1 to the plasma membrane at the site of bacterial entry. Nat Immunol 2010;11:55–62. [PubMed: 19898471]

52. Cadwell K, Liu JY, Brown SL, et al. A key role for autophagy and the autophagy gene Atg16L1 in mouse and human intestinal Paneth cells. Nature 2008; 456:259–263. [PubMed: 18849966]

53. Wang Y, Chiu CT, Nakamura T, et al. Elevated prolactin redirects secretory vesicle traffic in rabbit lacrimal acinar cells. Am J Physiol Endocrinol Metab 2007; 292:E1122–E1134. [PubMed: 17164431]

EDITOR'S NOTES

BACKGROUND AND CONTEXT

Exocytosis of zymogen granules and autophagy are two central processes for normal pancreatic acinar cell function and homeostasis, the dysregulation of which leads to pancreatic acinar cell injury resulting in pancreatitis.

NEW FINDINGS

SNARE protein Syntaxin-2 plays a paradoxical negative regulatory role in membrane fusion for exocytosis of zymogen granules and in preautophagosome growth. Syntaxin-2 deletion promoted basolateral exocytosis and increased autophagic vacuole formation with amplified zymogen activation within the autolysosomes.

LIMITATIONS

While Syntaxin-2 is susceptible to pancreatitis stimuli-induced protease degradation, that cellular protease is unknown, as is a specific protease inhibitor that could be used to abrogate pancreatic cell injury and alleviate pancreatitis.

IMPACT

Enhancing Syntaxin-2 levels or stability could be a therapeutic strategy to reduce aberrant exocytosis and dysregulated autophagy in pancreatic acini that could abrogate the progression to more severe pancreatitis.

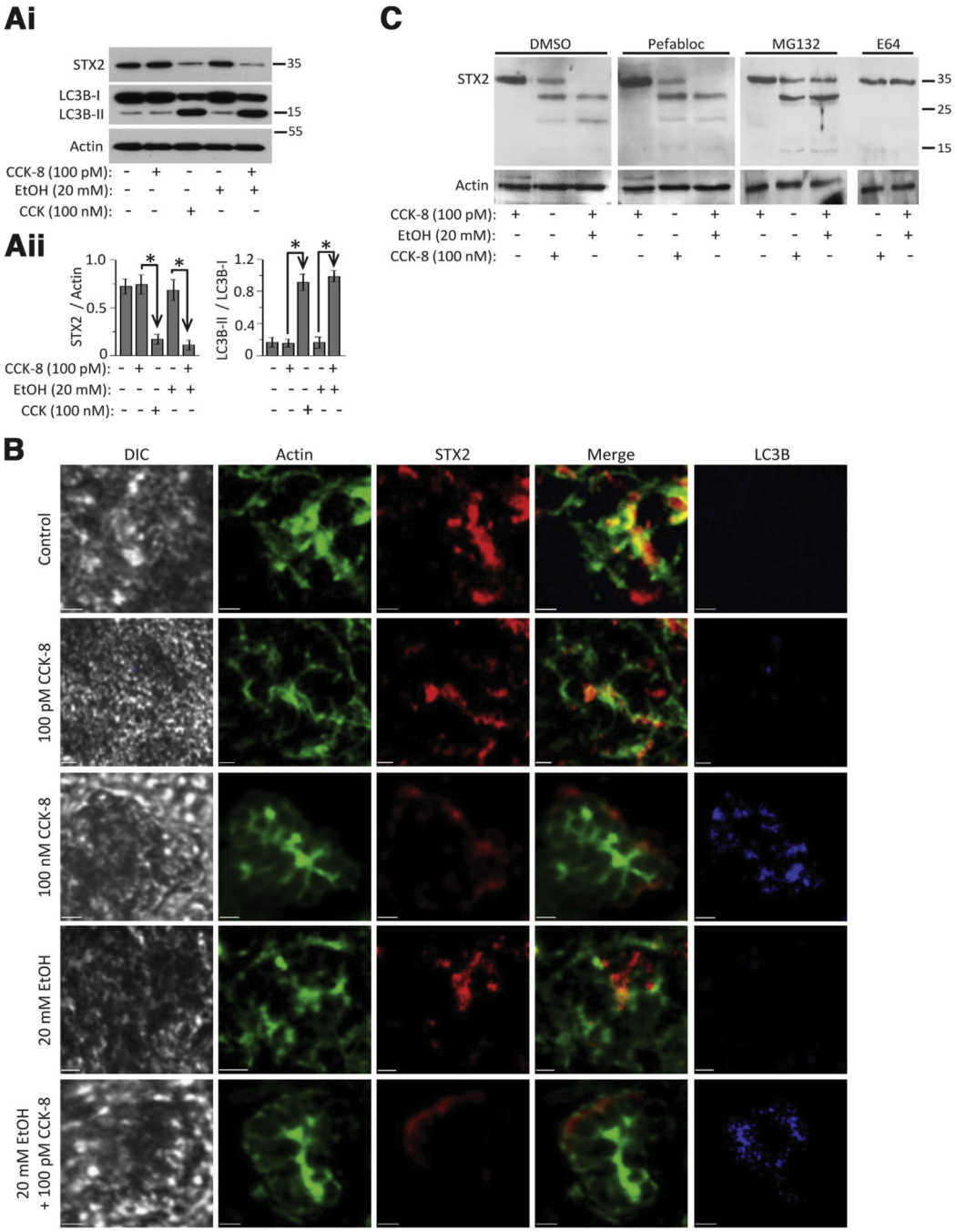

Figure 1.

Pancreatitis-inducing treatments promote STX2 cleavage by cystein protease and autophagy vacuole accumulation in human exocrine pancreas. Human pancreas slices (in extracellular solution (ECS) (*A*, *B*) were kept in basal conditions as control (ECS only) or 20 mM EtOH only, or stimulated with: 100 pM CCK (2 hours), supramaximal CCK (100 nM, 2 hours), or preincubated with 20 mM EtOH (1 hour) followed by 100 pM CCK (2 hours); all in 37°C. (*Ai*) Western blot analysis of lysates of human pancreas slices for STX2 and LC3B; actin as loading control. (*Aii*) Quantification of LC3B-II transition (densitometric ratio of LC3B-II

to LC3B-I) and STX2 (densitometric ratio of STX2 to actin) for human pancreas slices. (*B*) Representative immunofluorescence images of human pancreas slices probed for STX2, actin (phallodin), and LC3B (indicator of AVs). Differential interference contrast images show the intact pancreatic slice tissue. Merge images show abundance (or disruption) of STX2 in the apical PM, where actin is also most abundant. Another set of data are shown in Supplementary Figure 1F and 1G. (*C*) Representative Western blots from protease inhibitor screening for STX2 cleavage/degradation. Data are representative from 3 independent experiments. Scale bars = 20 μm. Analyses shown are mean ± SEM.

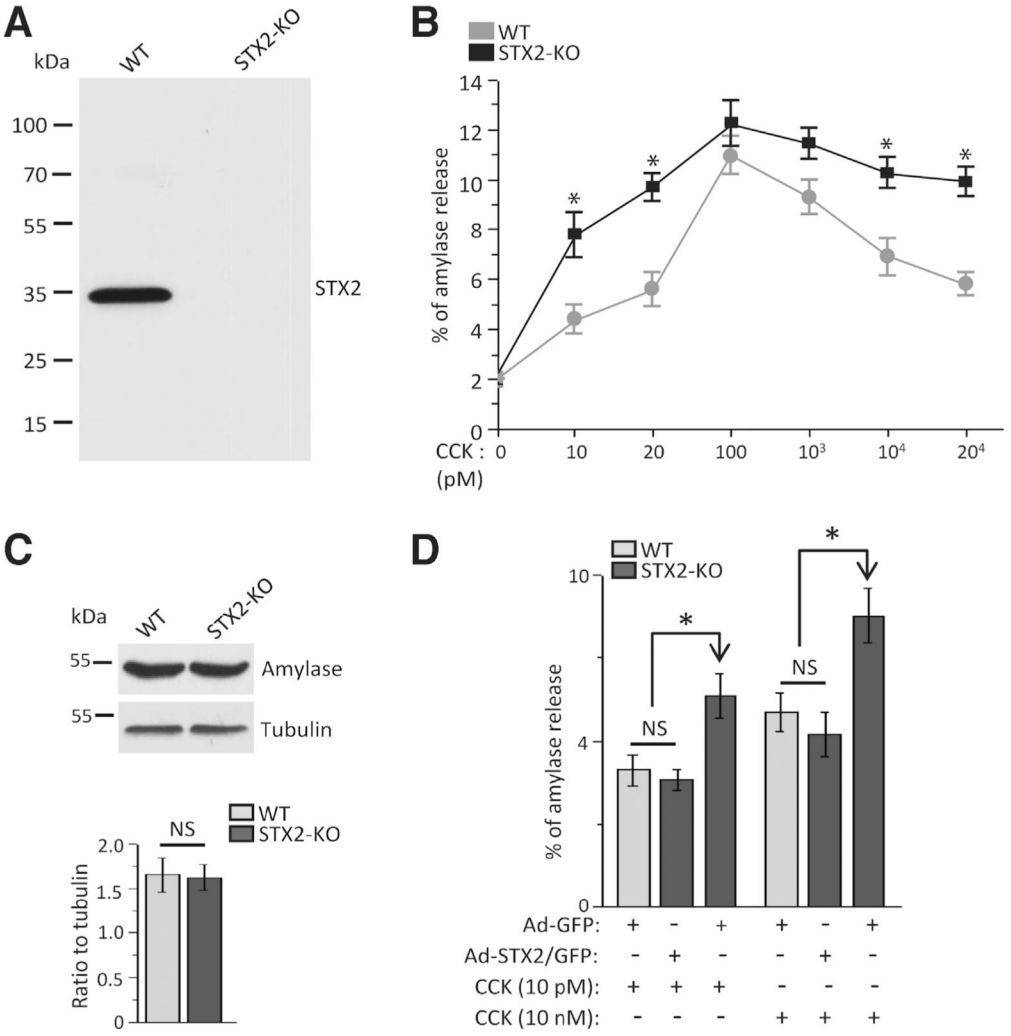

Figure 2.

STX2 deletion augments amylase secretion. (*A*) Representative Western blot (n = 3 independent experiments) showing complete absence of STX2 in STX2-KO acini. (*B*) STX2-KO (compared with WT) caused higher CCK-8 dose-dependent stimulated amylase secretion from dispersed pancreatic acini. Amylase released was expressed as percentage of total cellular amylase of the respective sample. n = 12 from 4 independent experiments. (*C*) Amylase expression (normalized to tubulin) showed no change between WT and STX2 KO acini. Three independent experiments. (*D*) Adenoviral expression of STX2/GFP into STX2-KO acini reduced the amplified secretory response to levels of WT acini (Ad-GFP infection). Amylase secretion quantified and expressed as in (*B*). Data shown represent mean ± SEM. **P* < .05; NS, not significant.

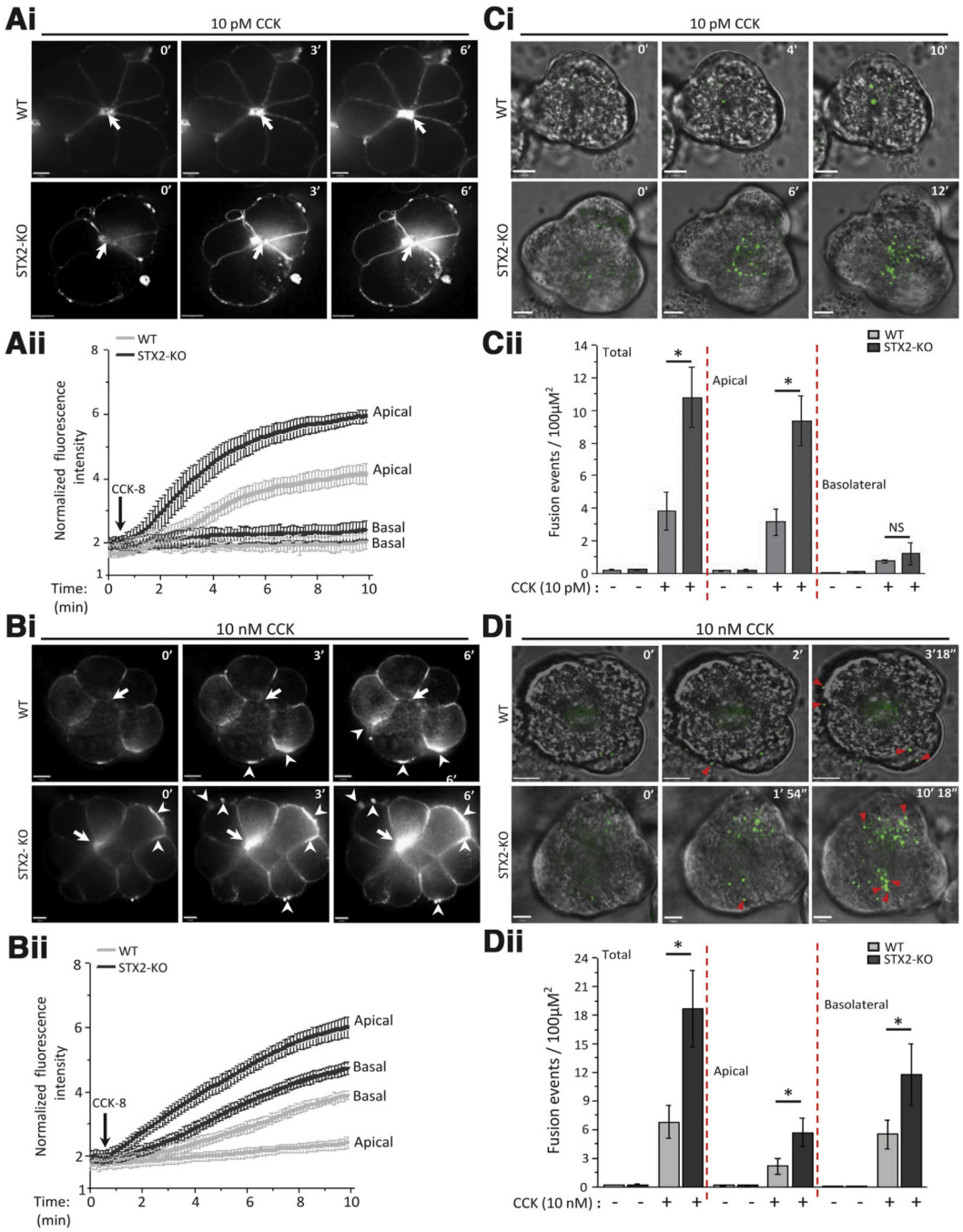

Figure 3.

STX2 deletion augments physiologic CCK-stimulated apical exocytosis and supraphysiologic CCK-stimulated pathologic exocytosis at the basal and lateral PM. (*Ai, Bi*) Sequences of FM1–43 exocytosis confocal images of freshly prepared acini from WT (*top*) and STX2-KO (*bottom*) mice stimulated with (*Ai*) 10 pM CCK-8 or (Aii) 10 nM CCK-8. Shown are representative images at the indicated time points (scale bar = 8 μm). FM1–43 exocytotic hotspots in apical ZG poles are indicated by *arrows,* and hotspots in basolateral pM are indicated by *arrowheads.* (*Aii, Bii*) Graphs are analysis (*Aii,* 10 pM CCK-8: WT-10

acini, STX2-KO-12 acini; *Bii,* 10 nM CCK-8: WT-9 acini, STX2-KO-10 acini; each from 3 independent experiments) of mean real-time fluorescent tracings of the apical versus basal PM normalized to basal intensity (before stimulation). (*Ci, Di*) Sequences (at indicated time points) of Ad-syncollin-pHluorin-transduced acini from WT (*top*) and STX2-KO (*bottom*) mice stimulated with (*Ci*) 10 pM CCK-8 or (*Di*) 10 nM CCK-8. Shown are representative images at indicated time points (clearer larger images in Supplementary Figure 3) and in real-time in movies (10 pM CCK-8: WT, Movie 1; STX2-KO, Movie 2; 10 nM CCK-8: WT, Movie 3; STX2-KO, Movie 4). Exocytosis toward lateral and basal PM is indicated by *red triangles.* (*Cii, Dii*). Graphs showing quantitative analysis (*Cii,* 10 pM CCK-8: WT-14 acini, STX2-KO-15 acini; *Dii,* 10 nM CCK-8: WT-12 acini, STX2-KO-16 acini; each from 5 independent experiments) of the fusion events at the apical and basolateral areas, and when combined as total. Apical and basolateral areas were divided by drawing 2 concentric circles centered on the apical lumen of each image where inner circle encompasses two-thirds of the area of the outer circle, and designated as “apical area.” Fusion events outside the apical area are considered “basolateral.”[22,29,53]

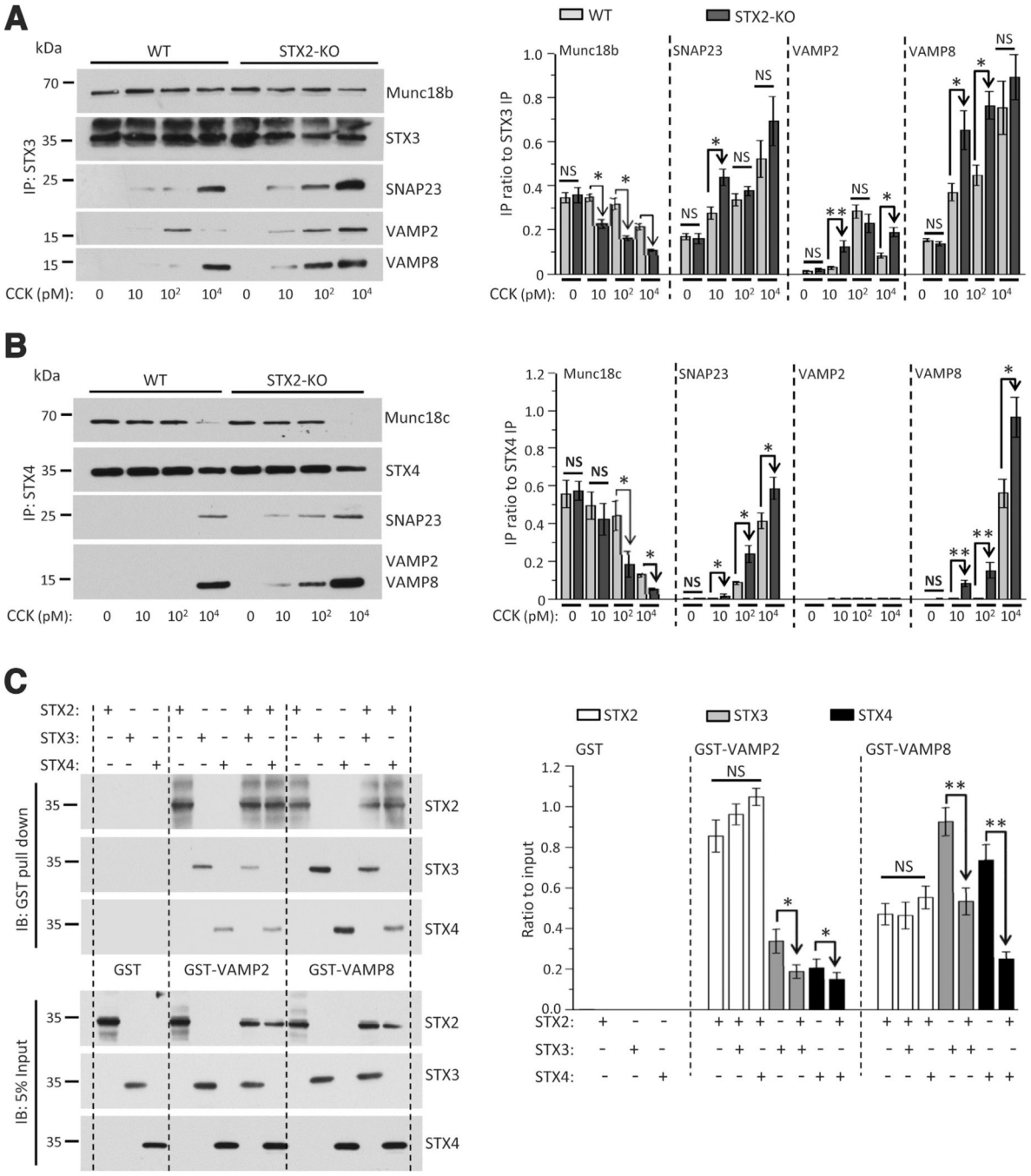

Figure 4.

STX2 deletion promotes STX3- and STX4-mediated SNARE complex assembly. Dispersed pancreatic acini from WT or STX2-KO mice were stimulated for 30 minutes with indicated doses of CCK-8, and then subjected to immunoprecipitation with antibodies against (*A*) STX3 or (*B*) STX4. Representative blots are shown in the *left panels.* Band intensity ratios of co-immunoprecipitated Munc18b/c, SNAP23, and VAMP8/2 relative to immunoprecipitated STX3 (*A*) or STX4 (*B*) are shown in corresponding *right panels,* expressed as ± SEM of 3 independent experiments. Five percent "input" controls (50 μg total acini lysates) with

densitometric analysis shown in Supplementary Figure 4A-D. (*C*) STX2 blocks STX3 and STX4 binding to cognate VAMP8 and VAMP2. STX2 is co-expressed with STX3 or STX4 in HEK cells; controls were expression of single STX and GST. HEK lysates were then subjected to pull-down with GST-VAMP8 or GST-VAMP2. Band intensity ratios of precipitated STX2, STX3 and STX4, and co-precipitated STX2/STX3, and STX2/ STX4 relative to the 5% inputs are shown in corresponding *right panels,* expressed as mean ± SEM of 3 independent experiments. $*P < .05$; $**P < .01$.

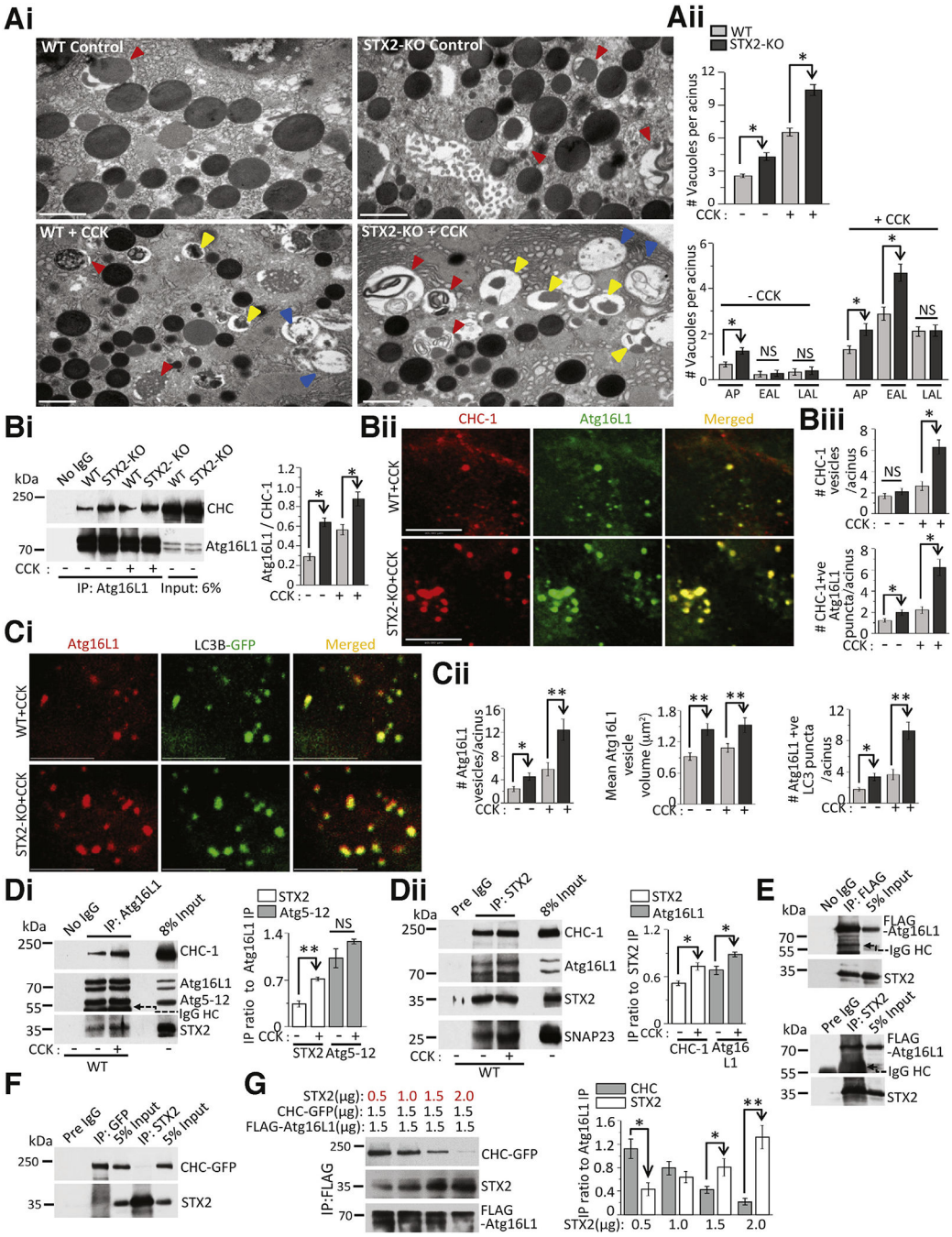

Figure 5.

STX2 deletion amplifies autolysosome accumulation by enhancing Atg16L1/CHC complex-mediated autophagosome formation. Unless otherwise stated, experiments were repeated 3 times; data shown are representative samples; analyses are mean ± SEM, *$P < .05$. (*Ai*) Transmission electron microscopy images depicting accumulation of distinct AVs (see description in Results), including APs (*red triangles*), EALs (*yellow triangles*), and late autolysosome (LAL, *blue triangles*) in control (*top panels*) or 30-minute 10 nM CCK-8-stimulated (*bottom panels*) WT or STX2-KO acini. Scale bars = 1 μm. (*Aii*) Quantification

of total (*top*) and individual (*bottom*) AVs. n = 60–70 acini. (*Bi*) Immunoprecipitation shows avid association of Atg16L1 with CHC-1 in STX2-KO acini. Thirty micrograms (6%) total cell lysates used as input. Quantification of Atg16L1 association with CHC-1 in *right.* (*Bii, Ci*) Confocal immunofluorescence images of selected areas showing (*Bii*) avid formation of clathrin and Atg16L1 vesicles and their colocalization, (*Ci*) avid formation of Atg16L1 vesicles and their incorporation into LC3B vesicles (APs) in STX2-KO acini on 10 nM CCK-8 stimulation. Full sequences of images with areas of interest (*boxed*) are in Supplementary Figure 5H. (*Biii*) Quantification of CHC-1 vesicles (*top*) and CHC-1-positive Atg16L1 vesicles (*bottom*). (*Cii*) Quantification of Atg16L1 vesicles from Bii and Ci (*left*), volume of Atg16L1 vesicles (*middle*) and Atg16L1-positive APs (*right*). (*Di, Dii*) Atg16L1 (*Di*) and STX2 (i) immunoprecipitations show Atg16L1/CHC-1/STX2 association. Forty micrograms (8%) total cell lysates used as input. Corresponding quantifications in *right.* (*E, F*) Immunoprecipitations of FLAG/STX2 (*E*) and STX2/CHC-GFP (*F*) show physical interaction between co-expressed (HEK293) FLAG-Atg16L1/STX2 (*E*), but not between CHC-GFP/STX2 (*F*). Twenty-five micrograms (5%) total cell lysates used as input. (*G*) STX2 dose-dependently blocks Atg16L1 association to CHC-1 association. Increasing amounts of STX2 co-expressed with constant amounts of Atg16L1-FLAG and CHC-1-GFP in HEK cells, then subjected to immunoprecipitation with anti-FLAG antibody; co-immunoprecipitated STX2 and CHC-1 band intensities analyzed as densitometry ratio to Atg16L1 (*right panel*). Five percent inputs shown in Supplementary Figure 5I. $*P < .05$; $**P < .01$.

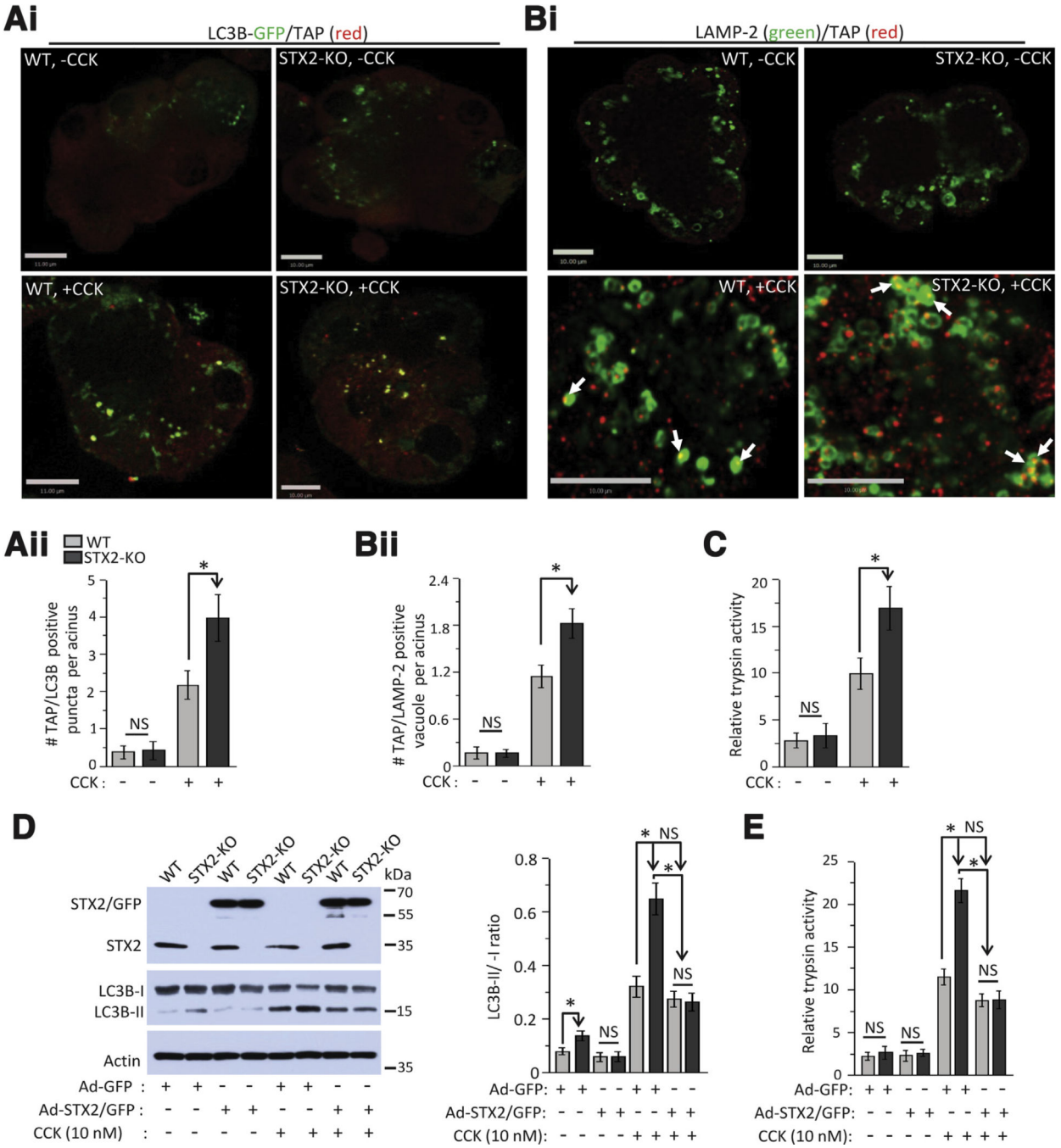

Figure 6.

STX2 deficiency promotes autolysosomal trypsinogen activation that could be abrogated by restoring STX2 expression. (*Ai*) Representative merged confocal images of LC3B-GFP and TAP in WT and STX2-KO acini transduced with Adeno-LC3B-GFP for 12 hours and then either kept as control (no CCK-8, *top panel*) or stimulated with 10 nM CCK-8 for 30 minutes (*bottom panel*) followed by probing with anti-TAP antibody. n = 3 independent experiments. Scale bars = 10 μm for WT, 11 μm for STX2-KO images. (*Aii*) Quantification of TAP-positive LC3B-GFP puncta from 80 acinar cells (at least 20 cells from each

experiment) from 3 independent experiments. Data expressed as mean ± SEM. (*Bi*) Representative merged confocal immunofluorescence images of LAMP-2 and TAP in WT and STX2 KO acini at control condition or stimulated with 10 nM CCK-8 for 30 min. Full sequence of images for (*A*) and (*B*) are shown in Supplementary Figure 7. (*Bii*) Quantification of TAP-positive LAMP-2 vacuoles from 50 acinar cells (at least 50 cells from each experiment) from 3 independent experiments. Data expressed as mean ± SEM. (*C*) Relative activity of trypsin in control and 10 nM CCK-8-stimulated WT and STX2-KO acini lysate. Data expressed as mean ± SEM from 3 independent experiments. (*D*) Adenoviral expression of STX2/GFP into STX2-KO acini abrogated the STX2 deletion-induced AV formation (LC3B-II conversion) and (*E*) intracellular trypsinogen activation. N = 3 independent experiments. Data expressed as mean ± SEM. $*P < .05$.

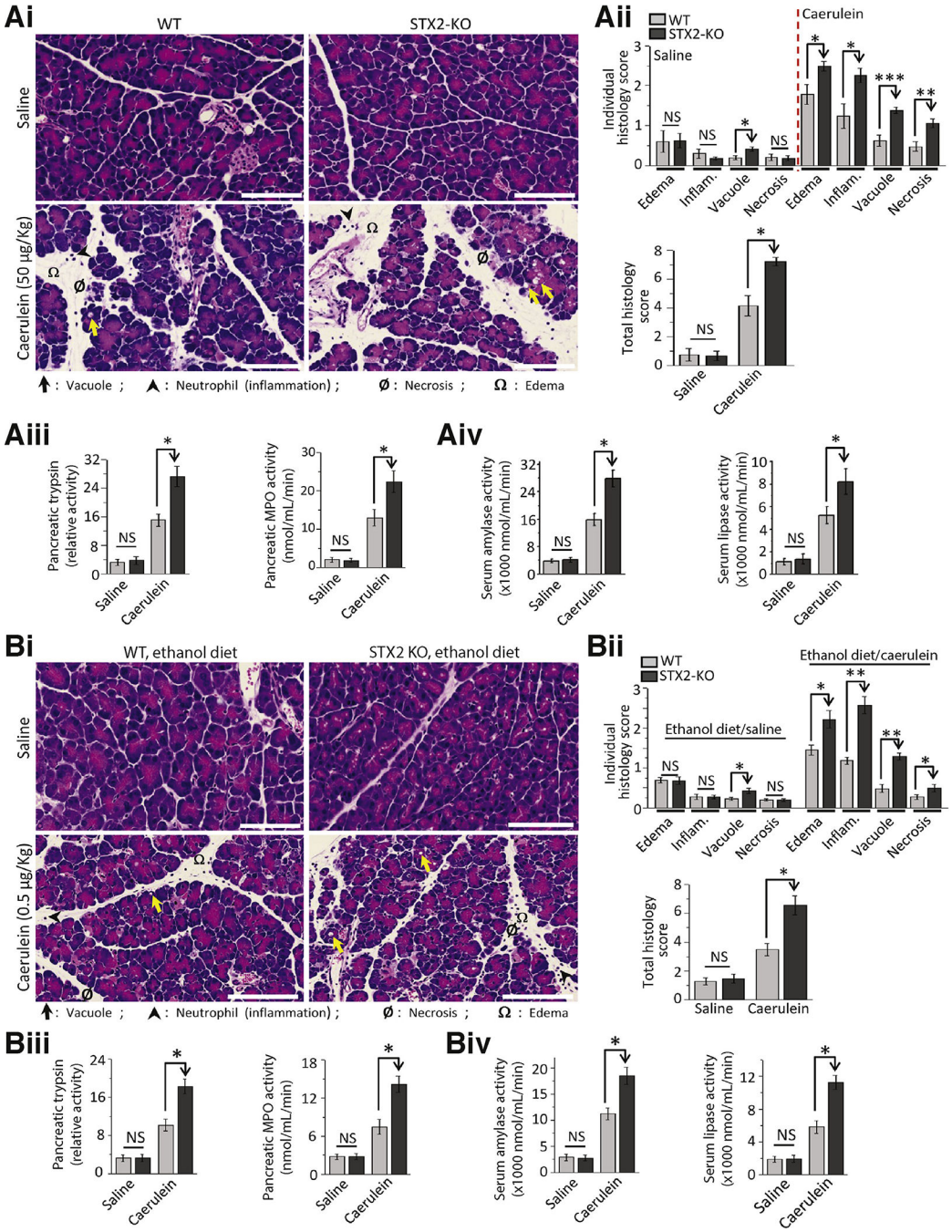

Figure 7.

STX2-KO mice are more susceptible to caerulein- and ethanol diet-induced pancreatitis. (*A*) Caerulein (n = 9 mice) and (*B*) ethanol fed (n = 8 mice) pancreatitis were induced in WT and STX2-KO mice, (*A*) supramaximal caerulein stimulation with 8 hourly intraperitoneal injections of 50 μg/kg caerulein. (*B*) 6-weeks ethanol feeding (36% of total calorie intake) followed by 5 hourly intraperitoneal injections of 0.5 μg/kg caerulein. Control mice (n = 4 each) in (*A*) and (*B*) were administered equal volume of 0.9% saline in parallel. Mice were sacrificed 1 hour after the last injection, then pancreatitis severity assessed. (*Ai, Bi*).

Representative H&E-stained images of pancreas from control (*top panels*) and pancreatitis-induced (*bottom panels*) mice (scale bar = 50 μm). Edema, inflammation, vacuolization, and necrosis are indicated by symbols at the bottom. (*Aii, Bii*) Individual (*top*) and combined histologic scoring (*bottom*) of edema, inflammation, vacuolization, and necrosis on a scale of 0–4 from pancreas of control or pancreatitis-induced mice. (*Aiii, Biii*) Relative activity of pancreatic trypsin (*left*) and quantitative measurements of pancreatic myeloperoxidase (MPO) activity (*right*). (*Aiv, Biv*) Serum levels of amylase (*left*) and lipase (*right*); all expressed as nmol/mL/min. Images are representative. Analyses are expressed as mean ± SEM from 3 independent experiments. *Enlarged histology images* in Supplementary Figure 7 show the pancreatic injury more clearly. NS, not significant. *$P < .05$; **$P < .01$; ***$P < .001$.